Coarsening kinetics of the bimodal γ′ distribution in DS GTD111™ superalloy

V. S. K. G. Kelekanjeri[1], S. K. Sondhi[2], T. Vishwanath[1], F. Mastromatteo[3] & B. Dasan[2]
[1]*GE Global Research Center, Materials Characterization Laboratory, Bangalore, India*
[2]*GE Global Research Center, Materials Research Laboratory, Bangalore, India*
[3]*GE Oil & Gas, Nuovo Pignone, Materials & Processing Engineering, Florence, Italy*

Abstract

Coarsening of γ′ precipitates in nickel-base superalloys is one of the mechanisms by which creep damage occurs in these alloys. This is brought about by a concomitant increase in the interparticle spacing, which results in faster dislocation movement and therefore, faster creep strain accumulation. Therefore, it is vital to accurately quantify the γ′ coarsening kinetics, which is essential for creep prediction via microstructure-based continuum damage mechanics models. In the present article, we report on coarsening studies of bimodally distributed γ′ precipitates in DS GTD111™ (Trademark of the General Electric Company).

The baseline microstructure of GTD111™ consisted of a cuboidal secondary γ′ population and a much finer, spherical tertiary γ′ population with respective mean radii of 266 and 34nm. Long-term aging experiments were conducted on baseline samples at temperatures of T1<T2<T3<T4 in the range of 800 to 1000°C. At T1, there was no clear trend in coarsening of the secondary γ′, likely due to interference effects from the tertiary distribution. Therefore, secondary γ′ coarsening was studied using data at higher temperatures where the distribution was clearly unimodal. The kinetics was extracted assuming the cubic rate law to be valid under conditions of volume diffusion controlled coarsening. Subsequently, the secondary γ′ kinetics was applied to predict coarsening of the tertiary distribution at T1 by incorporating a correction factor for volume fraction

WIT Transactions on Engineering Sciences, Vol 72, © 2011 WIT Press
www.witpress.com, ISSN 1743-3533 (on-line)
doi:10.2495/MC110221

enhancement of coarsening. Separately, the expected rate of tertiary γ′ coarsening was computed by compensating for volume fraction loss of tertiary γ′ between successive aging steps consumed during secondary γ′ coarsening. The coarsening rate constants from these two approaches were comparable. In summary, the present work is a treatment of bimodal γ′ coarsening kinetics in GTD111^{TM} where coarsening of the individual distributions are captured using a single consistent LSW rate equation.
Keywords: nickel-base superalloy, GTD111^{TM}, γ′ precipitate, γ-γ′ microstructure, bimodal distribution, coarsening, ostwald ripening, kinetics, creep, continuum damage mechanics.

1 Introduction

GTD111^{TM} is a directionally solidified nickel-base superalloy which is used in hot gas-path sections of gas turbines at temperatures of 750 to 800ºC [1]. The presence of a bimodal distribution of the γ′ ($Ni_3(Al,Ti)$) precipitate phase contributes to superior high temperature strength [2] of the alloy. However, upon prolonged thermal exposure, the γ′ distribution undergoes coarsening [3], resulting in an increase in the average interparticle spacing. This leads to easier movement of dislocations in the alloy and consequently, lower creep resistance [4]. In this context, γ′ coarsening as a damage mechanism warrants a detailed study so that an understanding of the kinetics of microstructure degradation may subsequently be used to develop continuum damage mechanics models.

Coarsening studies in multimodal precipitate systems has been reported in literature in both blade alloys such as GTD111 [5] and IN738 [6] and disc alloys such as Nimonic 115 [7] and Waspaloy [8]. Sharghi Moshatghin and Asgari [9] studied coarsening of bimodal γ′ distribution in IN738LC in terms of a compound size parameter that incorporates both primary and secondary γ′ dimensions. They found that the kinetics analyzed using this size parameter followed the cubic rate law in the range of 850 to 900ºC. Stevens and Flewitt [6] reported volume diffusion controlled coarsening kinetics for both secondary and tertiary γ′ in IN738 in the temperature range of 750 to 850ºC. Coakley et al. [7] implemented the numerical mean-field model based on the LSW theory, originally developed by Chen and Voorhees [10] to study bimodal γ′ coarsening in Nimonic 115. Experimental data at short aging durations behaved in accordance with the cubic rate law that corresponded to disappearance of the fine γ′ followed by a plateau region where the number of primary γ′ precipitates was nearly constant. At a later stage, data again followed the cubic rate law where coarsening was deemed to have reached steady-state. The numerical model predicted the trends in the experimental data reasonably well, better than the existing unimodal LSW coarsening models [7]. The present work involves experimental studies of γ′ coarsening in the temperature range of 800 through 1000ºC and subsequent treatment of bimodal γ′ coarsening kinetics using a single consistent LSW rate equation.

2 Experimental procedure

The baseline material for coarsening studies was GTD111™ which was solutionized at 1121°C for 2h followed by an inert gas fan cool and subsequently aged at 816°C for 4h. In order to conduct careful and thorough coarsening studies of GTD111™, baseline specimens, 20 in number, were first examined to obtain their key microstructural statistics, viz. secondary γ′ radius $\langle r_{S\gamma'} \rangle$, secondary γ′ volume fraction $f_{v\_S\gamma'}$, tertiary γ′ radius $\langle r_{T\gamma'} \rangle$ and volume fraction $f_{v\_T\gamma'}$. Subsequently, the baseline specimens were subjected to aging at temperatures of T1<T2<T3<T4 in the range of 800 to 1000°C up to 4000h. The specimens were again examined after conclusion of the aging treatments to extract the key microstructural parameters mentioned above.

The procedure for obtaining γ′ precipitate statistics comprised the sequence of metallography, microscopy and image analysis. Specimens were polished to mirror finish in the sequence of 220 grit diamond disc, 9μm, 3μm and 1μm diamond suspensions followed by colloidal silica suspension. Next, the as-polished specimens were etched using a solution comprising HCl, HNO_3 and H_2O and molybdic acid reagent. This etchant provides γ-γ′ contrast by preferentially dissolving the γ′ precipitate phase. Specimens were then examined in a scanning electron microscope and representative images of the underlying microstructure were acquired from dendritic cores. The images were then analyzed using customized image analysis routines to gather quantitative microstructural information.

3 Results

The baseline microstructure consisted of a bimodal distribution of cuboidal secondary γ′ precipitates and much finer tertiary γ′ precipitates as shown in fig. 1(a). The corresponding bimodal size distribution (PSD) is shown in fig. 1(b). The averaged baseline statistics from examination of 20 specimens are as follows:

$$\langle r_{S\gamma'} \rangle = 266\text{nm},\ f_{v\_S\gamma'} = 37\%,\ \langle r_{T\gamma'} \rangle = 34\text{nm and } f_{v\_T\gamma'} = 4\%.$$

The microstructures of specimens that are obtained upon aging will be summarized next. At T1, the microstructure consisted of a bimodal γ′ distribution after 250h of aging as seen from the micrograph in fig. 2(a). Upon further aging to 4000h, the microstructures did not show any significant coarsening of the secondary γ′ distribution (see fig. 2(b)); only a shape change from cuboids to corner-rounded cuboids was noted after 2000h of aging. The number density of tertiary precipitates decreased with progressive coarsening, also evident from the micrographs. At T2, the tertiary distribution was only sighted at 200h (see fig. 2(a)), beyond which, the tertiary precipitates coarsened and merged with the secondary PSD. Furthermore, shape change of the secondary precipitates from

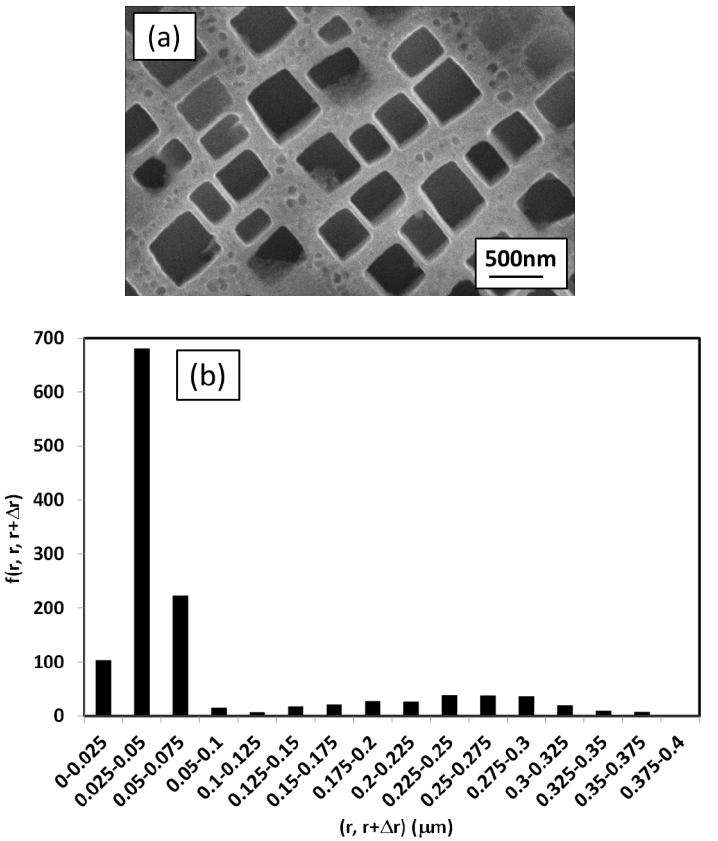

Figure 1: (a) Micrograph of GTD111^{TM} baseline specimen showing bimodal γ′ distribution and (b) histogram of the precipitate distribution.

corner-rounded cuboids to completely rounded shapes and accompanying coarsening was clear beyond 800h of aging. A micrograph representative of the microstructure at 4000h is shown in fig. 2(d) where rounded γ′ shapes are evident. The kinetics of coarsening was progressively faster at T3 and T4 due to which, snapshots of tertiary γ′ coarsening could not be captured even at relatively small aging durations of 100h.

A plot of the total and secondary γ′ volume fraction versus aging temperature is shown in fig. 3 for the aged specimens and the corresponding baselines. It is clear from the plot that f_{v_tot} is higher after aging, which is primarily due to discrepancy in the secondary γ′ volume fractions before and after aging. This unexpected rise in the volume fraction upon aging, across the temperature range of 800 to 1000°C is hard to reconcile because the thermodynamically permissible γ′ volume fraction resulting from the standard aging treatment should be higher

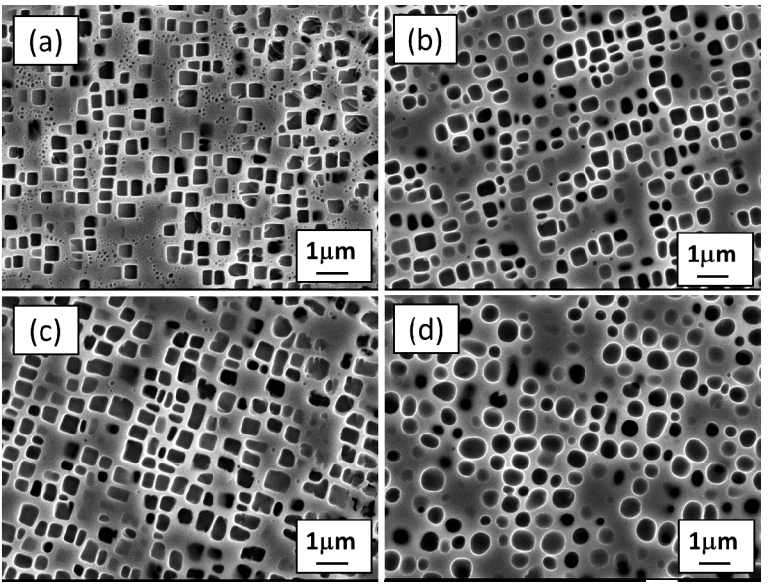

Figure 2: Representative microstructures of specimens aged for (a) 250h at T1, (b) 4000h at T1, (c) 200h at T2 and (d) 3200h at T2.

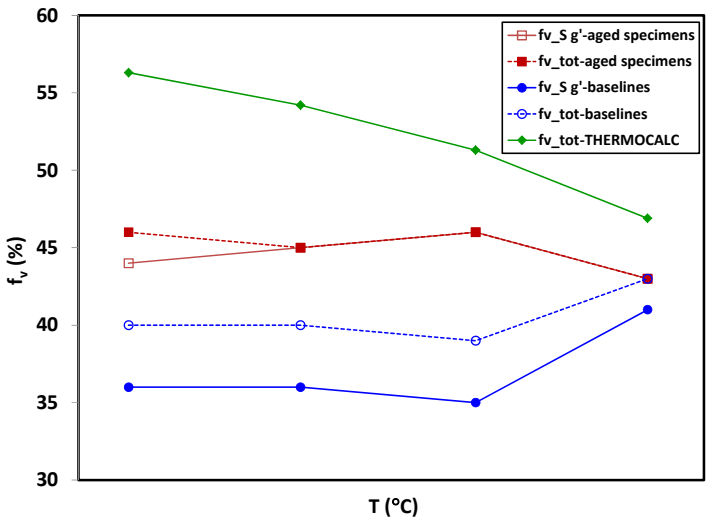

Figure 3: Plot of the secondary and total γ′ volume fractions in the baseline and aged specimens at temperatures of T1<T2<T3<T4. The expected trend in the equilibrium γ′ volume fraction (computed using THERMOCALC) through this temperature range is also shown.

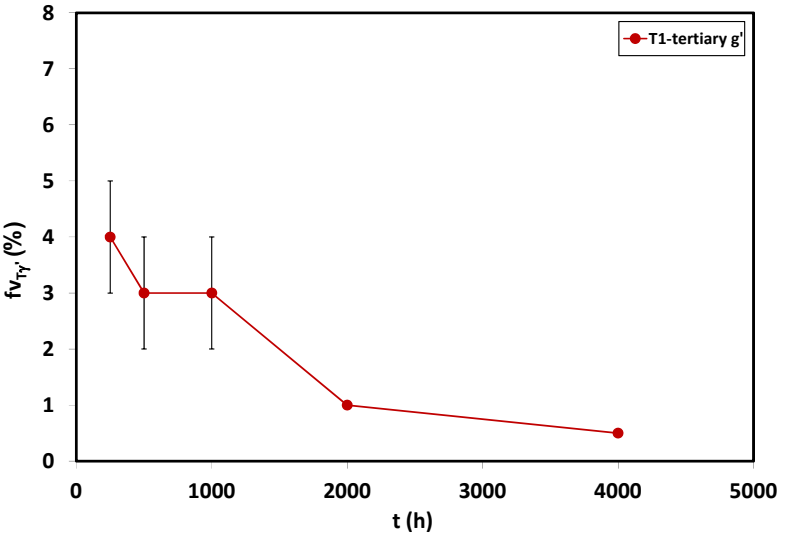

Figure 4: Plot showing evolution of the tertiary γ′ volume fraction at T1.

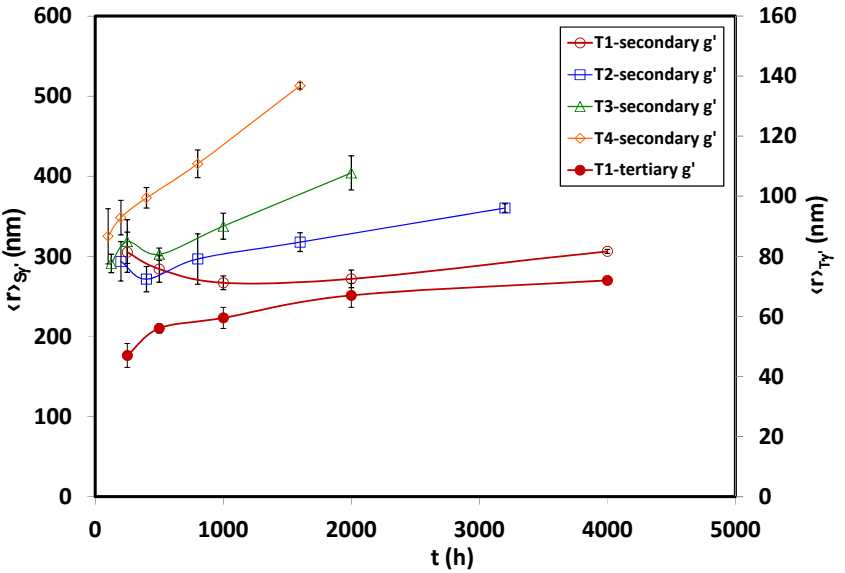

Figure 5: Plot showing evolution of the mean secondary γ′ radius with aging through temperatures of T1 through T4 (T1<T2<T3<T4). The variation of the mean tertiary γ′ radius at T1 is plotted on the secondary y-axis.

than at temperatures of T2 to T4. The latter is inferred from the monotonically decreasing trend in the THERMOCALC predicted equilibrium volume fraction

with increasing temperature, also shown in fig. 3. The evolution of the tertiary γ′ volume fraction upon aging at T1 is shown in fig. 4. The gradually decreasing trend is expected for two reasons- (a) consumption of the tertiary γ′ by the secondary γ′ during coarsening and (b) inherent coarsening of the tertiary γ′, thus merging with the secondary population.

Figure 5 shows a plot of the mean secondary γ′ radius versus aging time for all the four data sets. The expected increase in $\langle r_{S\gamma'} \rangle$ due to coarsening is preceded by a dip early on at T1, T2 and T3. The likely reason for this is attributed to fraction of the coarser tertiary population joining into the secondary distribution. The increase in the mean tertiary γ′ radius at T1 is also shown in the same plot. However, the observed increase in $\langle r_{T\gamma'} \rangle$ is apparent because of the fact that a fraction of the tertiary population is consumed during coarsening of the secondary distribution (see fig. 4), which otherwise would have participated in inherent coarsening of the tertiary distribution.

4 Analysis and discussion

The assumptions made for analysis of the coarsening kinetics using the results presented in the preceding section are stated as follows:

1. The baseline statistics need further validation because of the unexpected increase in the secondary and total γ′ volume fraction upon aging, as mentioned earlier. Therefore, coarsening analysis will be conducted using population statistics of the aged specimens only.
2. The kinetics of secondary γ′ coarsening will be analyzed using unimodal secondary γ′ statistics at T2, T3 and T4 after disappearance of the tertiary γ′ distribution. This ensures that any effects of the tertiary distribution on coarsening of the secondary population are no longer present. Therefore, the commencement of coarsening ($t = 0$) is defined as the earliest aging sampling step at which, the tertiary distribution is non-existent. Longer aging durations are accordingly shifted as per this definition. Data at T1 is not used for this analysis because a bimodal γ′ distribution is evidently present up to 4000h of aging. Furthermore, the present data do not show a clear coarsening trend in secondary γ′ size and γ′ statistics at longer aging times must be considered for obtaining a clearer trend.
3. The expected rate of coarsening of the tertiary γ′ distribution at T1 should be faster than the observed rate for reasons specified earlier. Therefore, to arrive at the expected coarsening rate, the loss of tertiary γ′ volume fraction between successive aging steps (see fig. 4) is reconciled and accounted for during coarsening.

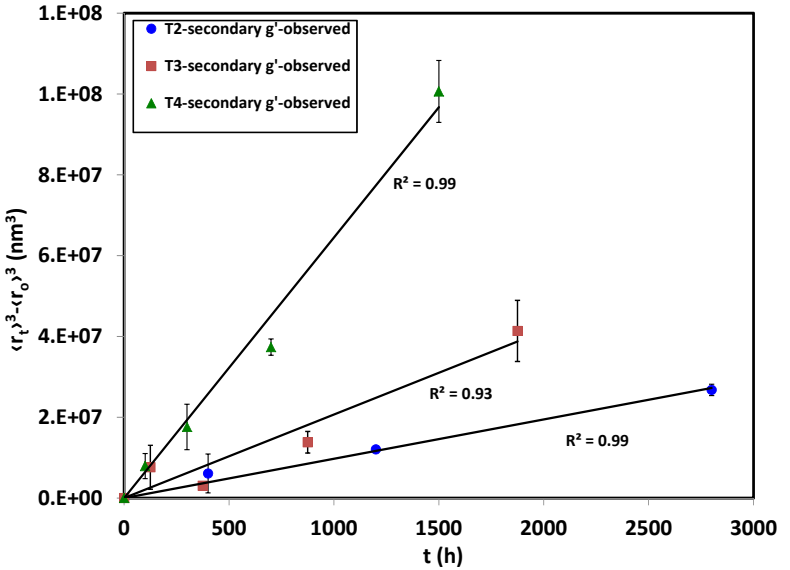

Figure 6: Cubic rate law plot of the mean secondary γ′ radius at T2, T3 and T4 (T2<T3<T4). Data used for analyzing kinetics correspond to unimodal secondary γ′ PSD's only.

As per assumption#2, secondary γ′ coarsening kinetics is analyzed using the cubic rate law $\left\langle r_{S\gamma'}^{t}\right\rangle^{3} - \left\langle r_{S\gamma'}^{o}\right\rangle^{3} = k(T)t$, where $\left\langle r_{S\gamma'}^{t}\right\rangle$ is the secondary γ′ radius at time t, $\left\langle r_{S\gamma'}^{o}\right\rangle$ is the radius at $t = 0$ and $k(T) = \frac{k_o}{T} e^{-\frac{Q}{RT}}$ is the coarsening rate constant with pre-exponential k_o and activation energy Q. A plot of the cubic rate law at T2, T3 and T4 shows reasonably good linear fits at all the three temperatures as shown in fig. 6. As expected and congruent with microscopic observations, the rate of coarsening (slope of the linear fit) is enhanced with increasing aging temperature. Next, a plot of the coarsening rate constant $k(T)$ versus $\left(\frac{1}{RT}\right)$ (see fig. 7) is used to extract the activation energy of coarsening as 212.45 (kJ/mol). The expression for the rate constant describing the secondary γ′ coarsening kinetics is as follows:

$$k(T) = \frac{k_o}{T} e^{-\frac{212447}{RT}} \text{ (nm}^3\text{/h)} \quad (1)$$

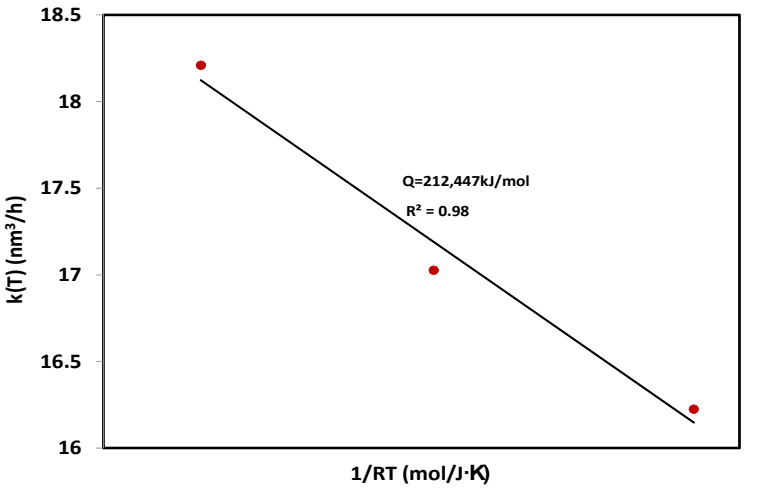

Figure 7: Plot of $k(T)$ vs. $\left(\frac{1}{RT}\right)$ using the rate constants at T2, T3 and T4. The activation energy of secondary γ′ coarsening is obtained as slope of the linear fit.

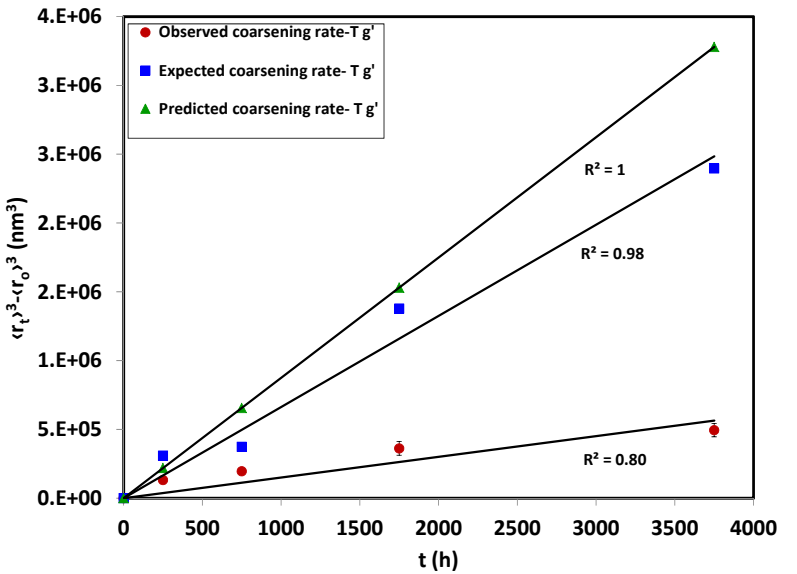

Figure 8: Cubic rate law plots of the mean tertiary γ′ radius at T1 shown for three cases – measured data, predicted dataset using secondary γ′ kinetics and expected dataset by correcting for volume fraction loss of tertiary γ′ during coarsening.

Next, this rate constant equation is used to predict coarsening of the tertiary γ′ distribution at T1 starting at 250h. However, realizing that eqn. (1) represents coarsening rate of the secondary γ′ distribution with a volume fraction of ~0.45, the enhanced coarsening rate due to high γ′ volume fraction [3,11,12] must be accounted for prior to applying the rate equation to the tertiary distribution. The pre-exponential in eqn. (1) is divided by a scaling factor $k(f_v) = 3.5$ to correct for volume fraction effects on coarsening [3]. The resulting equation for the rate constant, listed below, may then be applied to coarsening under low γ′ volume fraction scenario such as tertiary γ′ coarsening.

$$k(T) = \frac{0.29k_o}{T} e^{-\frac{212447}{RT}} \text{ (nm}^3\text{/h)} \tag{2}$$

Figure 8 shows a plot of $\left\langle r_{T\gamma'}^{t} \right\rangle^3 - \left\langle r_{T\gamma'}^{o} \right\rangle^3$ vs. t for tertiary γ′ coarsening at T1 and the corresponding linear fits for three cases – (a) 'observed' using measured data, (b) 'predicted' using eqn. (2) and (c) 'expected' by correcting measured data. The aging duration of 250h is taken to be the starting point i.e. $t = 0$ and the corresponding tertiary γ′ statistics are used to generate the predicted data set. The expected tertiary γ′ radii are computed in accordance with assumption#3 by the following procedure. Denote $f_{v\_T\gamma'}^{t_N}$, $N_{v\_T\gamma'}^{t_N}$ and $\left\langle r_{T\gamma'}^{t_N} \right\rangle$ to be the volume fraction, particle density (number of γ′ precipitates per unit volume) and mean radius of the tertiary γ′ distribution at the N^{th} aging time step corresponding to time $t = t_N$. It should be noted that the data point at 250h is denoted using the superscript t_o ($t_o = 0$ in this case) and longer aging times are scaled with reference to 250h as the starting point. Now, $\left(f_{v\_T\gamma'}^{t_{N-1}} - f_{v\_T\gamma'}^{t_N}\right)$ is the tertiary γ′ volume fraction which is consumed during secondary γ′ coarsening. This lost fraction between successive time steps is accounted for to obtain the expected γ′ radii. Specifically, the lost volume fraction $\left(f_{v\_T\gamma'}^{t_{N-1}} - f_{v\_T\gamma'}^{t_N}\right)$ results in a volume $\Delta V^{t_{N-1} \to t_N}$ over and above the volume $\left\langle V_{T\gamma'}^{t_N} \right\rangle$ of a tertiary γ′ precipitate with mean size $\left\langle r_{T\gamma'}^{t_N} \right\rangle$. The quantities $\left\langle V_{T\gamma'}^{t_N} \right\rangle$ and $\Delta V^{t_{N-1} \to t_N}$ are defined as below:

$$\left\langle V_{T\gamma'}^{t_N} \right\rangle = \frac{4}{3}\pi \left\langle r_{T\gamma'}^{t_N} \right\rangle^3 \tag{3}$$

and

$$\Delta V^{t_{N-1} \to t_N} = \frac{\left(f_{v\_T\gamma'}^{t_{N-1}} - f_{v\_T\gamma'}^{t_N}\right)}{N_{v\_T\gamma'}^{t_N}} \tag{4}$$

Here $N_{v\_T\gamma'}^{t_N}$ is the number density of tertiary γ′ precipitates at the instant $t = t_N$. Using this framework, the expected mean tertiary γ′ radius $\left\langle r_{\exp ected\_T\gamma'}^{t_N} \right\rangle$ at $t = t_N$ is computed as:

$$\left\langle r_{\exp ected\_T\gamma'}^{t_N} \right\rangle = \left[\frac{\left\langle V_{T\gamma'}^{t_N} \right\rangle + \sum_{1}^{N} \Delta V^{t_{N-1} \to t_N}}{\left(4/3\,\pi\right)} \right]^{1/3} \tag{5}$$

The correlation coefficient of the linear fit is improved from 0.8 for the measured data to 0.98 (see fig. 8) for the 'expected' data set by making this correction. The agreement between the coarsening rate constants of the 'expected' and 'predicted' datasets is also better when compared to the rate constant of the measured dataset. The reasons for disparity between the rate constants of the 'expected' and 'predicted' data sets could be two fold. First, there could be errors associated with truncation of the tertiary PSD due to overlap of the secondary and tertiary distributions, as is the case at 1000 and 2000h at T1. Secondly, any variations in the γ′ precipitate statistics that exist among the baselines are ignored in the present analysis. It is quite possible that the truncation errors and initial baseline variations could lead to errors in estimation based on eqn. (5).

5 Conclusions

Aging experiments were conducted on GTD111™ in the temperature range of 800 to 1000°C with the objective of studying bimodal γ′ coarsening kinetics in this alloy. Secondary γ′ coarsening kinetics elucidated using data where the PSD's were clearly unimodal yielded an activation energy of 212.45 (kJ/mol). This kinetics was then applied to tertiary γ′ coarsening at the lowest aging temperature by using an appropriate scaling factor to discount volume fraction enhancement of coarsening. Separately, the kinetics of the measured data was corrected approximately by accounting for volume fraction loss of tertiary γ′ between successive aging steps accompanying secondary γ′ coarsening. The coarsening rate constants obtained from these two approaches showed a reasonable agreement with each other. Thus, the kinetics of bimodal γ′ coarsening in GTD111™ could be described using a single consistent LSW rate equation in the chosen range of temperatures.

Acknowledgements

The authors greatly appreciate S. Vipin for careful metallographic preparation of GTD111™ aged specimens. Next, we would like to acknowledge the staff at the National Metallurgical Laboratory, Jamshedpur, India for their assistance in

characterization of the baseline GTD111™ specimens. We also acknowledge the helpful discussions with Drs. M. Karadge and S. Swaminathan on treatment of coarsening data.

References

[1] Schilke, P. W. *Advanced gas turbine materials and coatings.* GE Energy. Schenectady, NY : s.n.

[2] Sims, C. T. and Hagel, W. C. *The Superalloys.* New York : John Wiley & Sons, 1972.

[3] Martin, J. W., Doherty, R. D. and Cantor, B. *Stability of microstructure in metallic systems.* New York : Cambridge University Press, 1997.

[4] Dyson, B., Use of CDM in materials modelling and component creep life-prediction. *ASME Journal of Pressure Vessel Technology*, **315**, pp. 281-296, 2000.

[5] Mastromatteo, F., Niccolai F., Giannozzi, M. and Bardi, U., The coarsening kinetic of γ' particles in nickel-based superalloys during aging at high temperatures. *Proceedings of the ASME Turbo Expo*. **4**, pp. 851-856, 2004.

[6] Stevens, R. A. and Flewitt, P. E. J., The effects of γ′ precipitate coarsening during isothermal aging and creep of the nickel-base superalloy IN-738. *Materials Science and Engineering A* **3**, pp. 237-247, 1979.

[7] Coakley, J., Basoalto, H. and Dye, D., Coarsening of a multimodal nickel-base superalloy. *Acta Materialia* **58**, pp. 4019-4028, 2010.

[8] Kelekanjeri, V. S. K. G., Moss, L. K., Gerhardt, R. A. and Ilavsky, J., Quantification of the coarsening kinetics of γ′ precipitates in Waspaloy microstructures with different prior homogenizing treatments. *Acta Materialia*, **57(16)**, pp. 4658-4670, 2009.

[9] Sharghi-Moshatghin, R and Asgari, S., The effect of thermal exposure on the γ′ characteristics in a Ni-base superalloy. *Journal of Alloys and Compounds* **368**, pp. 144-151, 2004.

[10] Chen, M. K. and Voorhees, P. W., The dynamics of transient Ostwald ripening. *Modelling and Simulation in Materials Science and Engineering*, **1(5)**, pp. 591-612, 1993.

[11] Davies, C. K. L., Nash, P. and Stevens, R. N., The effect of volume fraction of precipitate on ostwald ripening. *Acta Metallurgica*, **28(2)**, pp. 179-189, 1980.

[12] Voorhees, P. W. and Glicksman, M. E., Solution to the multi-particle diffusion problem with applications to ostwald ripening-II. Computer simulations. *Acta Metallurgica*, **32(11)**, pp. 2013-2030, 1984.